

# **Atomic Displacements due to Spin-Spin Repulsion in Conjugated Alternant Hydrocarbons**

Ernesto Estrada<sup>1</sup>, Michele Benzi<sup>2</sup>

<sup>1</sup>Department of Mathematics & Statistics, University of Strathclyde, Glasgow G11XQ, UK

<sup>2</sup>Department of Mathematics and Computer Science, Emory University, Atlanta, Georgia  
30322, USA

We develop a theoretical model to account for the spin-induced atomic displacements in conjugated alternant hydrocarbons. It appears to be responsible for an enlargement of the distance between pairs of atoms separated by two atoms and located at the end of linear polyenes. It also correlates very well with the bond dissociation enthalpies for the cleavage of the C-H bond as well as to the spin density at carbon atoms in both open and closed shell at graphene nanoflakes (GNFs). Finally, we have modified the Schrödinger equation to study the propagation of the spin-induced perturbations through the atoms of GNFs.

## 1. Introduction

Conjugated alternant hydrocarbons (CAHs) have played a fundamental role in the development of theoretical chemistry. The effectiveness of the Hückel molecular orbital (HMO) method for studying electronic properties of CAHs continues to amaze generations of chemists [1]. The whole area of chemical graph theory has been fueled by the development of theoretical tools for studying the energetic properties of conjugated polyenes and polycyclic aromatic compounds as well as fullerenes and carbon nanotubes [2, 3]. The recent discovery of graphene has increased the interest in CAHs in physics, chemistry and material sciences from both a theoretical and experimental perspective [4]. In particular, the existence of open-shell configurations in certain graphene nanoflakes (GNFs) has been identified as the major cause of relevant magnetic properties, such as in the case of trigonal zigzag GNFs which are predicted to show metallic antiferromagnetism [5, 6]. The same electronic property is also responsible for the intriguing properties of functionalized trigonal GNFs, such as spin transfer, their use as components in molecule-based conductors and as electrode active materials in secondary batteries [7]. Graphene nanoflakes (GNFs), also known as nanoislands or nanodisks, are finite-sized graphene fragments of arbitrary size and shape. When the edges of these fragments are passivated by hydrogen, GNFs are realizable as all-benzenoid PAHs [8] in which all carbon atoms have  $sp^2$  hybridization. GNFs can possess large spins depending of their shapes, which include linear, triangular, rectangular, parallelogrammic, hexagonal, bowtie, etc.

Apart from the well-known fact that the zero-energy states in CAHs give rise to unbonded electrons or radicals, any CAH can be represented as a superposition of various resonant structures which include a few radical ones. In other words, any CAH has a radicaloid structure even in the case that they do not have any zero-energy states [7, 9-13]. Such radical character is responsible for the nonlinear optical (NLO) properties of several

GNFs [11-13]. It is also expected to influence the spin density at the different sites of GNFs and consequently the electronic, optical and magnetic properties of GNFs.

In this work we propose a theoretical approach to account for the atomic displacements in CAHs due to spin-spin repulsions between pairs of atoms that are separated by two bonds. Our approach consists in considering the CAH as a quantum harmonic oscillator in which carbon atoms separated by two bonds are connected by springs with negative (repulsive) force constant. We then derive the thermal Green's function for this system which accounts for the atomic displacement due to the spin-spin repulsion between atoms which are separated by two bonds in alternant conjugated systems. Due to the bipartite nature of CAHs, the zero-energy states, if they exist, lie just in the middle of the spectrum of a CAH. The particular mathematical form of the thermal Green's function defined here gives more weight to those energy levels which are at the centre of the spectrum of the CAHs. Then, the atomic displacements due to spin-spin repulsion correlate very well with the spin density at the given atoms, which make them suitable descriptors for C-H bond dissociation enthalpies at these sites. More importantly, we have discovered a tiny effect in the geometry of linear conjugated polyenes reflected in their crystallographic structures which could be due to the atomic displacements induced by spin-spin repulsion. This effect is not accounted for by *ab initio* quantum chemical methods.

## 2. Theoretical Model

Let us consider an alternant conjugated hydrocarbon consisting of  $n$  carbon atoms connected through alternant double and single bonds. The molecule is then represented by a bipartite graph such that the carbon atoms can be divided into two subsets (starred and unstarred), in a way that any site from one subset has its neighbors only in the other subset. This implies that if  $E_j$  is an energy level of a CAH, then  $-E_j$  is also an energy level, with the

same multiplicity. In addition, according to the spin alternation rule [14-16], which states that the singlet spin pairing is preferred solely between sites in different subsets, the free valences on the starred and unstarred sites might be identified with “up” and “down” spin. Consequently, any pair of carbon atoms separated by two bonds has the same spin. This means that we can consider that pairs of atoms separated by two bonds in CAHs suffer spin-spin repulsion. Let us assume that every carbon atom is represented by a ball of mass  $m$  and that there is a spring with the spring constant  $-m\omega^2$  connecting two balls separated by two bonds. The negative sign of these spring constants indicates that there is repulsion between these pairs of atoms due to spin-spin interactions.

We now consider the CAH as a quantum harmonic system in which atoms oscillate under thermal disturbances. For the sake of simplicity, we assume that there is no damping and no external forces are applied to the system. The coordinates chosen to describe a configuration of the system are  $x_i$ ,  $i=1,2,\dots,n$ , each of which indicates the fluctuation of the atom  $i$  from its equilibrium point  $x_i=0$ . In order to find how the thermal disturbances propagate through the molecule we will start by considering a Hamiltonian of the form

$$H = \sum_i \left[ \frac{p_i^2}{2m} + (K_i - k_i) \frac{m\omega^2 x_i^2}{2} \right] - \frac{m\omega^2}{4} \sum_{i < j} T_{ij} (x_i - x_j)^2, \quad (1)$$

where  $k_i$  is the number of atoms adjacent to the atom  $i$  and  $K_i$  is a counter term that offsets the movement of the whole molecule by tying it to the ground. The second term of the right-hand side is the potential energy of the springs connecting the balls. The term  $T_{ij}$  is equal to one if the atoms  $i$  and  $j$  are separated by two bonds, or zero otherwise. The first term in the first set of square parentheses is the kinetic energy of the atom  $i$ . Here we consider  $K_i = 2k_i$  in (1) such that the Hamiltonian can be written as:

$$H = \sum_i \left[ \frac{p_i^2}{2m} + \frac{m\omega^2}{2} x_i^2 k_i \right] + \frac{m\omega^2}{2} \sum_{i,j} x_i T_{ij} x_j, \quad (2)$$

This Hamiltonian can then be simplified to

$$H = \sum_i \frac{p_i^2}{2m} + \frac{m\omega^2}{2} \sum_{i,j} x_i P_{ij} x_j, \quad (3)$$

where the entries of the matrix  $\mathbf{P}$  are

$$P_{ij} = \begin{cases} k_i & \text{if } i = j \\ 1 & \text{if } d_{ij} = 2 \\ 0 & \text{otherwise,} \end{cases} \quad (4)$$

and  $d_{ij}$  is the number of bonds separating the corresponding atoms.

It is straightforward to realize that the matrix  $\mathbf{P} = \mathbf{A}^2$ , where the adjacency matrix  $\mathbf{A}$  is a square symmetric matrix whose entries are ones or zeros if the corresponding pairs of atoms are bonded or not, respectively. It corresponds to the Hamiltonian of the Hückel molecular orbital (HMO) method [1].

Here we are interested only in the influence of the molecular topology in the propagation of the spin-spin repulsions between pairs of atoms separated by two bonds. Consequently, we can approximate the Hamiltonian in the following way

$$H \simeq \sum_{i,j} x_i P_{ij} x_j = \sum_{i,j} x_i \left( \mathbf{A}^2 \right)_{ij} x_j. \quad (5)$$

We now obtain the diagonal thermal Green's function  $G_{pp}(\beta)$ , where we have restricted ourselves to the space spanned by the ground state (the vacuum). This function indicates how much an excitation at a given carbon atom propagates through the whole molecule before coming back to the same atom and being annihilated,

$$G_{pp}(\beta) = \frac{1}{Z} \langle vac | a_p e^{-\beta H} a_p^\dagger | vac \rangle, \quad (6)$$

where  $\beta$  is the inverse temperature,  $Z$  is the partition function,  $a_p^\dagger$  and  $a_p$  are the creation and annihilation operators. Following the procedure described in [17] we obtain the thermal Green's function, which is given by

$$G_{pp}(\beta) = (e^{-\beta H})_{pp} = (e^{-\beta A^2})_{pp} = \sum_{j=1}^n \varphi_j^2(p) \exp(-\beta \lambda_j^2), \quad (7)$$

where  $\lambda_j$  is an eigenvalue of  $\mathbf{A}$  and  $\varphi_j$  its corresponding eigenfunction. In the current study we will keep  $\beta \equiv 1$  in all the calculations.

### 3. Spin-induced Atomic Displacements in Polyenes

In this section we develop some analytic expressions for  $G_{pp}$  in linear and cyclic polyenes. A linear polyene is represented by a path graph. That is, a graph in which every node is adjacent to other two except two nodes which are adjacent to only one node. The  $p$ th entry of the  $j$ th eigenvector of the adjacency matrix of  $P_n$  is given by

$$\varphi_j(p) = \sqrt{\frac{2}{n+1}} \sin \frac{jp\pi}{n+1} \quad (j=1, \dots, n) \text{ and the corresponding eigenvalue by } \lambda_j = 2 \cos \frac{j\pi}{n+1}$$

[18]. Then we have

$$G_{pp} = \frac{2}{n+1} \sum_{j=1}^n \sin^2 \left( \frac{jp\pi}{n+1} \right) e^{-4 \cos^2 \left( \frac{j\pi}{n+1} \right)}. \quad (8)$$

By using trigonometric relationships this expression can be modified to

$$\begin{aligned} G_{pp} &= \frac{2}{n+1} \sum_{j=1}^n \left[ \frac{1}{2} - \frac{1}{2} \cos \left( \frac{2jp\pi}{n+1} \right) \right] e^{-4 \cos^2 \left( \frac{j\pi}{n+1} \right)} \\ &= \frac{e^{-2}}{n+1} \left[ \sum_{j=1}^n e^{-2 \cos^2 \left( \frac{2j\pi}{n+1} \right)} - \sum_{j=1}^n \cos \left( \frac{2jp\pi}{n+1} \right) e^{-2 \cos^2 \left( \frac{2j\pi}{n+1} \right)} \right]. \end{aligned} \quad (9)$$

Let

$$G'_{pp} = \frac{e^{-2}}{\pi} \left[ \int_0^\pi e^{-2\cos\theta} d\theta - \int_0^\pi \cos(2\theta p) e^{-2\cos\theta} d\theta \right], \quad (10)$$

and let

$$I_0(z) = \frac{1}{\pi} \int_0^\pi e^{\pm z \cos\theta} d\theta, \quad (11)$$

$$I_k(z) = \frac{1}{\pi} \int_0^\pi e^{\pm z \cos\theta} \cos(k\theta) d\theta, \quad (12)$$

be Bessel functions of the first order. Then,

$$G'_{pp}(P_n) = e^{-2} \left[ I_0(2) - I_{r(p)}(-2) \right], \quad (13)$$

where

$$r(p) = \begin{cases} p & \text{if } p \leq n/2 \text{ (} n \text{ even) or } p \leq (n+1)/2 \text{ (} n \text{ odd)} \\ n-p+1 & \text{if } p > n/2 \text{ (} n \text{ even) or } p > (n+1)/2 \text{ (} n \text{ odd),} \end{cases}$$

and  $\theta = \pi j / (n+1)$ . Finally, we can see that  $G_{pp}(P_n) / G'_{pp}(P_n) \rightarrow 1$  as  $n \rightarrow \infty$ .

A cyclic polyene can be represented by a cycle graph, which is the one in which every node is adjacent to other two. Here we consider only cyclic polyenes of even length, otherwise they are not bipartite. Following an analogous procedure as the previously described we find that

$$G'_{pp}(C_n) = e^{-2} I_0(2), \quad (14)$$

where also  $G_{pp}(C_n) / G'_{pp}(C_n) \rightarrow 1$  as  $n \rightarrow \infty$ .

As an example we illustrate in the following Table the values of  $G_{pp}$  for the atoms  $p=1,\dots,4$  in octatetraene,  $P_8$  (see Figure 1). The atoms are labeled as in Figure 1. For the cyclooctatetraene or [8]annulene ( $C_8$ ) the value of  $G_{pp}$  is 0.3022 while that obtained by using formula (15) is 0.3085.

**Insert Table 1 and Figure 1 about here.**

The study of polyenes demonstrates that the degree of connectivity of a given atom is an important factor in determining the atomic displacements due to spin-spin repulsion. That is, the terminal  $CH_2$  groups have more atomic displacements than the  $CH$  groups at the centre of the chain. As a consequence the separation between the atoms labeled as 1 and 3 in linear polyenes is expected to be larger than those for pairs more at the centre of the chain, such as atoms 2 and 4 or 3 and 4'. Due to the weak nature of the spin-spin repulsion this effect is expected to be relatively small. However, the X-ray structure of all-trans 1,3,5,7-octatetraene reveals that this effect is observed for the different pairs of atoms separated by two bonds in the molecule (see Table 2) [19]. For instance, the distance between the atoms 1 and 3 in this molecule is 2.469 Å, which is slightly longer than that between the atoms 2 and 4 (2.466 Å). The distance between atoms 3 and 4' is again slightly enlarged with respect to that of the pair 2-4 (2.468 Å). Such alternancy cannot be explained by effects in the crystal structure. However, it is predicted by our current model as can be seen in Table 1 where we give the sum of the atomic displacements between the corresponding pairs of atoms as an indication of the effect of the spin-spin repulsion between atoms separated by two bonds. It is worth mentioning here that this effect is not reproduced by high-level *ab initio* quantum chemical calculations as can be seen in Table 1 [20]. In all the cases reported the distance between atoms 1 and 3 is shorter than those of the atoms 2-4 and 3-4'. Consequently, we argue here

that the consideration of the weak spin-spin repulsion between pairs of atoms separated by two bonds could be a desirable correction for quantum chemical approaches.

**Insert Table 2 about here.**

#### **4. Spin-induced Atomic Displacements in Graphene Nanoflakes**

Another factor which is expected to influence  $G_{pp}$  is the radical character of the corresponding atom. It is expected that the larger the radical density in a given atom, the larger the atomic displacement due to spin-spin repulsion. Here we study computationally the atomic displacement due to spin-spin repulsion in graphene nanoflakes. First we start by studying how  $G_{pp}$  can give information about physicochemical properties of the atoms in these molecules, which indirectly can provide hints about the relation between the atomic displacements and spin densities. We then analyze the relation between  $G_{pp}$  and the bond dissociation enthalpies (kcal/mol at 298K) for the cleavage of the C-H bond in PAHs. In Figure 2 we show the mean atomic displacements due to spin-spin repulsion at the nonequivalent sites of naphthalene, anthracene and pyrene together with their bond dissociation enthalpies calculated at the B3LYP/6-31G(d) level by Barckholtz et al. [21]. For naphthalene we also shown the experimental values reported by Reed and Kass [22]. As can be seen the  $G_{pp}$  index perfectly predicts the sites with the largest enthalpies for cleavage the C-H bond, which correspond to those with the highest mean atomic displacement due to spin-spin repulsion.

**Insert Figure 2 about here.**

In order to understand this result we first need to understand the relation between the atomic displacements and the density of radicals at given atoms. If we consider two atoms separated by two bonds the repulsion force acting on them is basically due to the spin-spin

repulsion. Then, if the spin densities at such atoms are large the repulsion between the atoms should be stronger. In closing, the atomic displacement should be larger for those pairs of atoms displaying high spin densities. The spin density is expected to be higher at those sites in which radicals or radicaloids are localized. Consequently, we expect a correlation between the radical density at a given site and the atomic displacement due to spin-spin repulsion. Now we can understand why the sites with the largest atomic displacements are those with the highest bond dissociation enthalpies. That is, the site with the largest  $G_{pp}$  is also that with the largest radical (spin) density. Then removing the hydrogen attached to this site is quite energetic as it will increase dramatically the radical density at this carbon atom.

Now we study the atomic displacements due to spin-spin repulsion of four types of GNF systems, namely: linear (acenes), hexagonal (coronenes), trigonal (triangulenes) and bowtie GNFs. The first two types of systems are examples of closed-shell GNFs and the last two represent systems with open-shells. As can be seen in Figure 3 for small representatives of the GNFs studied here the index  $G_{pp}$  predicts the largest atomic displacements at the edges of the GNFs in a way that coincides with the spin densities calculated for these systems using first principle methods [9]. This is a remarkable finding as our Hamiltonian does not consider electron spin explicitly. It can be interpreted by considering that the carbon sites where certain radicaloid structures exist suffer the largest spin-spin repulsion and so their atomic displacements are relatively large. In the case of the triangulene illustrated in Figure 3 the sites with the largest atomic displacements are those that support radicals in the molecules obtained experimentally so far. For instance, the derivative of triangulene reported by Allison et al. in 1995 [23] displays the radicals at the three sites in which  $G_{pp}$  is maximum. A similar observation holds for the derivative obtained by Inoue et al. in 2001 [24]. All these findings indicate that the index  $G_{pp}$  is a good indicator of the spin density at sites in GNFs.

**Insert Figures 3 about here**

Finally, we consider the atomic displacements entropy in order to study the total atomic displacements delocalization in the GNFs studied. It is defined as  $S = -\sum_i p_i \ln p_i$ , where  $p_i = \exp(-\beta\lambda_i^2) / Z$ . We then study the average entropy per site  $\langle S \rangle$ . The results indicate that the maximum atomic displacement per site is present in the hexagonal system. At the same time the highest localization is obtained for the triangular GNF, with the linear and bowtie GNFs occupying an intermediate position:  $\langle S \rangle_H = 11.4$ ,  $\langle S \rangle_L = 11.2$ ,  $\langle S \rangle_B = 11.1$  and  $\langle S \rangle_T = 10.7$ . The highest localization in the triangular system is expected from the fact that it has an open shell configuration in which a few radicals are found in some sites with high probability. The same is also expected for the bowtie nanoflake, which indeed has the second largest localization according to  $\langle S \rangle$ . The surprise then comes from the similarity in the localization index between the linear system and those with open-shell configurations. Despite the fact that linear GNFs are expected to have closed shell configurations, there are important clues that when the number of fused rings is larger than 7 the ground states of these nanoflakes are antiferromagnetic ones [25-27], which agrees with our prediction about the similarity between this system and the open-shell ones.

## **5. Propagation of spin-induced perturbations**

Now, let us consider how the perturbation produced at the site  $x_0$  by the spin-spin repulsion propagates through the whole molecule. If we consider that such perturbation is located at this atom at the time  $t = 0$ , the dynamics of the propagation through the sites of the molecule can be understood by studying the evolution of the electronic wave packet given by the time-dependent Schrödinger equation with the Hamiltonian (5) ( $\hbar = 1$ )

$$i \frac{\partial \psi(t)}{\partial t} = A^2 \psi(t), \quad (15)$$

with the initial condition  $\psi_x(t=0) = \delta_{x,x_0}$ . The solution of (4) is  $\psi(t) = \exp(-itA^2)\psi(0)$ .

Obviously, the amplitude that the perturbation that resided at site  $q$  at time  $t=0$  ends up at the site  $p$  due to the quantum dynamics is given by  $\langle p | \exp(-itA^2) | q \rangle$ . Then, by continuation from the real time  $t$  to the imaginary time, we obtain the thermal Green's function as  $G_{pq} = \langle p | \exp(-\beta A^2) | q \rangle$ .

In order to compare the dynamic properties of the four systems under study we analyze the scaling behavior of the temporal autocorrelation function averaged over different nonequivalent initial positions of the wave packet. The temporal autocorrelation function is defined by  $C(t) = \left\langle \frac{1}{t} \int_0^t |\Upsilon_{pp}(t')|^2 dt' \right\rangle$ , where  $\Upsilon_{pq}(t) = \left[ \exp(-itA^2) \right]_{pq}$  and  $\langle \dots \rangle$  indicates the average over the nonequivalent sites. The integrand of this function  $P_p(t) = |\Upsilon_{pp}(t)|^2$  is known as the return probability of the wave packet initially localized at the site  $p$ . It is known that the temporal autocorrelation function scales as  $C(t) \sim t^{-\delta}$ , where  $0 \leq \delta \leq 1$  [28]. As it is well known  $\delta=0$  indicates localization of the wave packet,  $0 < \delta < 1$  indicates anomalous diffusion and  $\delta=1$  indicates ballistic motion. Thiem and Schreiber [29] have recently suggested the use of the scaling behavior of the return probability instead of that of the autocorrelation function. In this case,  $P(t) \sim t^{-\delta'}$  and it is expected that  $\delta' = \delta$ . However, it is usually the case that  $\delta' > \delta$  and  $\delta'$  can be even larger than one, which according to Zhong and Mosseri [30], makes the integral in the autocorrelation function convergent, yielding  $C(t) \sim 1/t$ . In Figure 4 we illustrate the scaling behavior of the return probability and the temporal autocorrelation function for the four systems studied. The sizes of the systems are

498, 486, 526, and 500, respectively. It is observed in the four GNF systems that  $C(t)$  decays with a power-law behavior before approaching a constant value due to finite size effects. The quantity  $C(t)$  decays strongly for the GNFs with closed-shell systems, i.e., linear and hexagonal, indicating a more extended nature of the wave functions in these systems. That is, the values of  $\delta$  for the four systems are, respectively  $\delta_H = 0.92$ ,  $\delta_L = 0.92$ ,  $\delta_B = 0.89$  and  $\delta_T = 0.88$ , where H, L, B and T stand for hexagonal, linear, bowtie and triangular, respectively. This indicates that in the four systems there is anomalous quantum diffusion with larger localization of the radical wave packet in those systems with open-shells. In general, it is difficult to extract the scaling behavior for the return probability in these systems due to the short period of decay before the wave packet starts to oscillate around a constant value due to the small sizes of the systems considered here. The only exception is the linear GNF where it was possible to check that  $P(t) \sim t^{-1.02}$ , indicating a ballistic motion of the radical along the linear graphene nanostructure. Therefore, the same kind of ballistic motion should be expected for the hexagonal system.

**Insert Figure 4 about here.**

## 6. Conclusions

We consider a conjugated alternant hydrocarbon as a network of quantum harmonic oscillators. Instead of considering bonded atoms as connected by springs here we assume that pairs of atoms separated by two bonds are connected by springs of negative constant. This repulsive effect arises from the spin-spin repulsion between these atoms which have the same spin. Using this model we derive the atomic displacements due to spin-spin repulsion as the thermal Green's function of a network of quantum harmonic oscillators. Then, we show that the spin-induced atomic displacement is responsible for: (i) an enlargement of the distance between pairs of atoms separated by two atoms and located at the end of linear polyenes; (ii)

bond dissociation enthalpies for the cleavage of the C-H bond at different sites of polycyclic aromatic hydrocarbons; (iii) the spin density at carbon atoms in both open and closed shell graphene nanoflakes (GNFs). Finally, we use a modified Schrödinger equation to study the propagation of the spin-induced perturbations through the atoms of GNFs.

### **Acknowledgement**

EE acknowledge the University of Strathclyde New Professor's Fund and MB thanks the National Science Foundation, grant DMS1115692, for partial financial support.

## References

- [1] W. Kutzelnigg, *J. Comput. Chem.* 28 (2007) 25-34.
- [2] M. Randić, *Chem. Rev.* 103 (2003) 3449-3605
- [3] A.T. Balaban, *Phys. Chem. Chem. Phys.* 13 (2011) 20649-20658
- [4] A.K. Geim, *Science* 324 (2009) 1530-1534.
- [5] M. Esawa, *Phys. Rev. B* 76 (2007) 245415.
- [6] O.V. Yazyev, *Rep. Prog. Phys.* 73 (2010) 056501.
- [7] Z. Sun, J. Wu, *J. Mater. Chem.* 22 (2012) 4151-4160.
- [8] I. Gutman, J. Brunvoll, *Advances in the theory of benzenoid hydrocarbons II.* Springer-Verlag, Berlin, 1992.
- [9] J.S. Murray, F. Abu-Awwad, P. Politzer, *J. Mol. Struct. (Theochem)* 501-502 (2000) 241-250.
- [10] F.A. Bulat, J.S. Burgess, B.R. Matis, J.W. Baldwin, L. Macaveiu, J.S. Murray, P. Politzer, *J. Phys. Chem. A* 116 (2012) 8644-8652.
- [11] K. Yoneda, M. Nakano, R. Kishi, H. Takahashi, A. Shimizu, T. Kubo, K. Kamada, K. Ohta, B. Champagne, E. Botek, *Chem. Phys. Lett.* 480(2009) 278-283.
- [12] H. Nagai, M. Nakano, K. Yoneda, H. Fukui, T. Minami, Se. Bonness, R. Kishi, H. Takahashi, T. Kubo, K. Kamada, K. Ohta, B. Champagne, E. Botek, *Chem. Phys. Lett.* 477 (2009) 355-359.
- [13] H. Nagai, M. Nakano, K. Yoneda, R. Kishi, H. Takahashi, A. Shimizu, T. Kubo, K. Kamada, K. Ohta, E. Botek, B. Champagne, *Chem. Phys. Lett.* 489 (2010) 212-218.
- [14] S.N. Natta, P. Mukherjee, P.P. Jha, *J. Phys Chem. A* 107 (2003) 5049-5057.
- [15] J.A. Chan, B. Montanari, J.D. Gale, S.M. Bennington, J.W. Taylor, N.M. Harrison, *Phys. Rev. B* 70 (2004) 041403R.
- [16] E.H. Lieb, *Phys. Rev. Lett.* 62 (1989) 1201-1204.

- [17] E. Estrada, N. Hatano, M. Benzi, *Phys. Rep.* 514 (2012) 89-119
- [18] E. Estrada, *The Structure of Complex Networks*. Oxford University Press, 2011.
- [19] R.H. Baughman, B.E. Kohler, I.J. Levy, C. Spangler, *Synth. Met.* 11 (1985) 37-52.
- [20] V. Schettino, F.L. Gervasio, G. Cardini, P.R. Salvi, *J. Chem. Phys.* 110 (1999) 3241-3250.
- [21] C. Barckholtz, T.A. Barckholtz, C.M. Hadad, *J. Am. Chem. Soc.* 121 (1999) 491-500.
- [22] D.R. Reed S.R. Kass *J. Mass Spectrom.* 35 (2000) 534–539
- [23] G. Allinson, R.J. Bushby, J.-L. Paillaud, M. Thornton-Pett, *J. Chem. Soc. Perkin Trans. 1* (1995) 385-390.
- [24] J. Inoue, K. Fukui, S. Nakazawa, K. Sato, D. Shiomi, Y. Morita, K. Yamamoto, T. Takui, K. Nakasuji, *J. Am. Chem. Soc.* 123 (2001) 12702-12703.
- [25] D. Jiang, S. Dai, *J. Chem. Phys. A* 112 (2008) 332-335.
- [26] Z. Qu, D. Zhang, C. Liu Y. Jiang, *J. Phys. Chem A* 113 (2009) 7909-7914.
- [27] S. Motomura, M. Nakano, H. Fukui, K. Yoneda, T. Kubo, R. Carion, B. Champagne, *Chem. Phys. Phys. Chem.* 13 (2011) 20575-20583.
- [28] R. Ketzmerick, G. Petschel, T. Geisel, *Phys. Rev. Lett.* 69 (1992) 695-698.
- [29] S. Thiem and M. Schreiber, [ArXiv:1204.4211v1](https://arxiv.org/abs/1204.4211v1).
- [30] J. Zhong, R. Mosseri, *J. Phys.: Cond. Matt.* 7 (1995) 8383.

## Table and Figure captions

Table 1. Exact values of the thermal Green's function for the nonequivalent atoms in octatetraene as well those calculated by using formula (14). The labeling of the atoms is given in Figure 1.

Table 2. Atomic distance between pairs of atoms separated by two bonds in octatetraene obtained from x-ray crystallography as well as calculated by different *ab initio* methods. The values of the sum of the atomic displacements  $G_{pp} + G_{qq}$  due to spin-spin repulsion are also given.

Figure 1. Illustration of the atomic displacements in octatetraene,  $G_{pp}$ . The circles radii are proportional to the values of the displacements and the colors are used to differentiate atoms in each partition of the bipartite graph.

Figure 2. Illustration of the atomic displacements due to spin-spin repulsion,  $G_{pp}$  and the bond dissociation enthalpies (kcal/mol at 298K) for the cleavage of the C-H bond at different sites of three PAHs. The atomic displacements due to spin-spin repulsion are plotted as circles whose radii are proportional to  $G_{pp}$  and the color correspond to spin up or down. Values in parenthesis are obtained experimentally by Reed and Kass [22].

Figure 3. Illustration of the atomic displacements due to spin-spin repulsion at the sites of some small representatives of the four types of GNFs studied. The atomic displacements are plotted as circles whose radii are proportional to  $G_{pp}$  and the color correspond to atoms in the same bipartite set.

Figure 4. Scaling behavior of the return probability and the temporal autocorrelation function for the dynamics of spin-induced perturbations in the four types of GNFs studied in this work.



Table 1

atom	exact	Formula (14)
1	0.5238	0.5238
2	0.2153	0.2153
3	0.3371	0.3373
4	0.3030	0.3016

Table 2

Method	$d_{13}$	$d_{24}$	$d_{34}$
Exp.	2.469	2.466	2.468
HF/6-31G*	2.464	2.466	2.465
MP2/6-31G*	2.468	2.476	2.473
6-31G	2.468	2.471	2.468
B3LYP/6-31G*	2.471	2.481	2.478
$G_{pp} + G_{qq}$	0.861	0.518	0.674

Figure 1

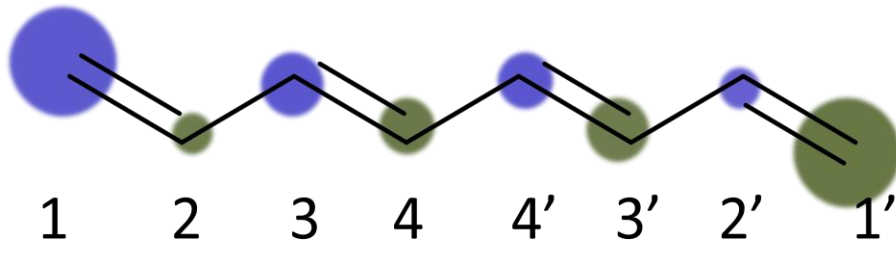


Figure 2

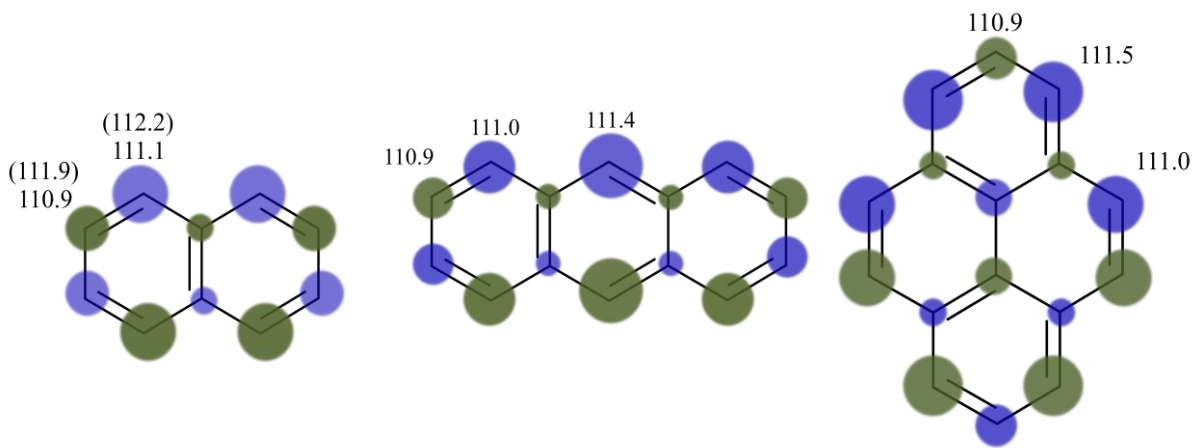


Figure 3

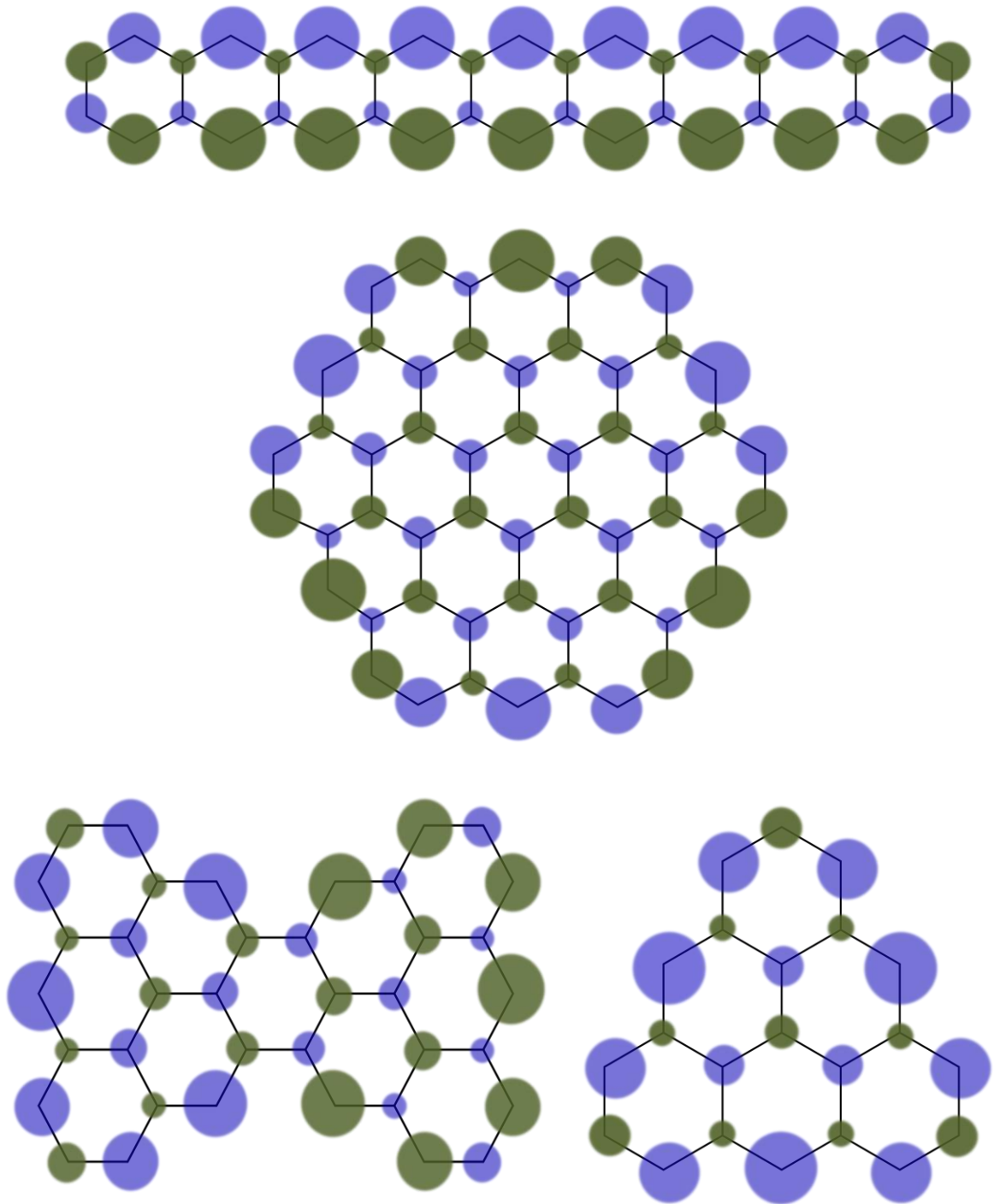
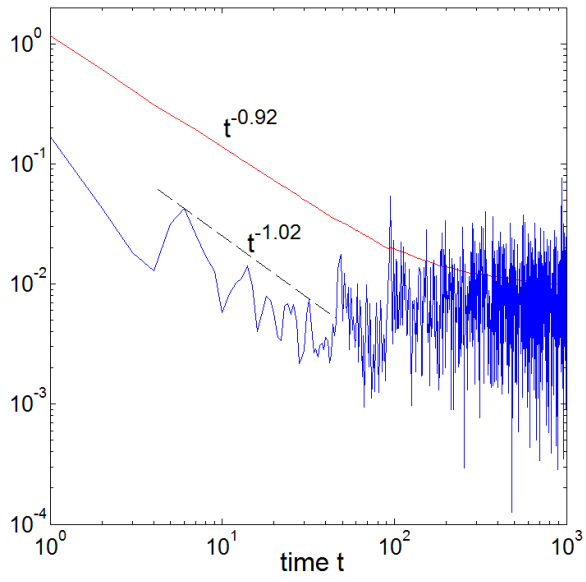
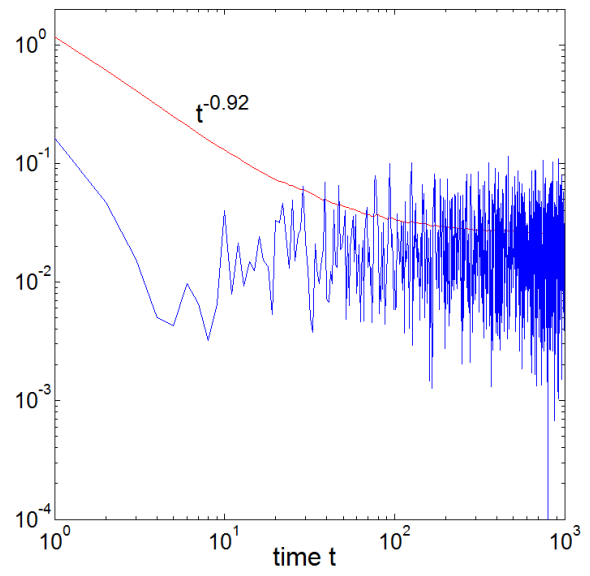


Figure 4

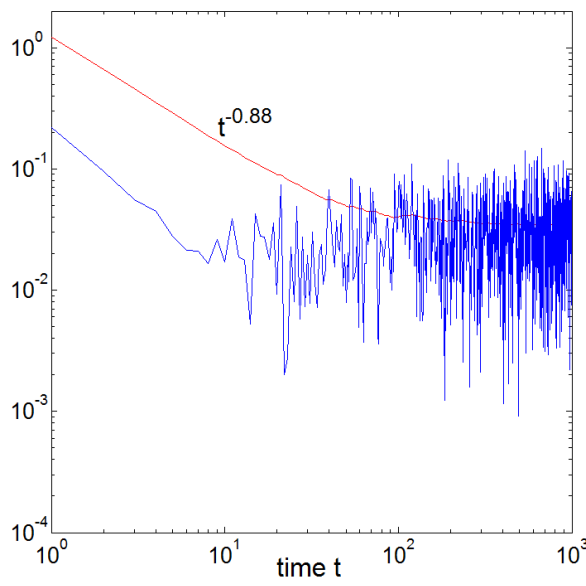
Linear



Hexagonal



Triangular



Bowtie

